metals

MDPI

Article

Effect of Microstructure on the Precipitation of β-Mg_2Si during Cooling after Homogenisation of Al-Mg-Si Alloys

Endre Hennum [1], Knut Marthinsen [2,*] and Ulf H. Tundal [1]

[1] Hydro Aluminium AS, N-6601 Sunndalsøra, Norway; endre.hennum@hydro.com (E.H.); ulf.tundal@hydro.com (U.H.T.)
[2] Department of Materials Science and Engineering, Faculty of Natural Sciences, Norwegian University of Science and Technology, N-7491 Trondheim, Norway
* Correspondence: knut.marthinsen@ntnu.no; Tel.: +47-41513972

Abstract: For Al-Mg-Si alloys, cooling after homogenisation is a crucial step because the precipitation of the equilibrium β-Mg_2Si phase determines the processing capabilities in subsequent steps, as well as the subsequent precipitation age hardening potential, and thus, the final properties. It is therefore important to understand how microstructural variations affect the transformation of β-Mg_2Si during cooling after homogenisation. In the present work, alloys with similar effective solute contents of Mg and Si, but with different microstructures and a different amount of primary Al-Fe-Si phases, were produced. Characterisation of the precipitation reaction was performed using interrupted quench experiments with cooling rates of 1–6 K/min, monitored by light optical microscopy (LOM), scanning electron microscopy (SEM) and conductivity measurements. Precipitation kinetics for β-Mg_2Si was found to increase in microstructures with shorter secondary dendrite arm spacing (DAS). However, despite measuring both a higher density and volume fraction of the primary phases, no effect on the phase transformation from an increased iron content was found in terms of precipitation kinetics or particle count statistics. Furthermore, comparisons with iron-free high-purity-based alloys revealed that the precipitation reaction for β-Mg_2Si was identical in the two different microstructures both in terms of onset temperature and overall kinetics. The present results show that nucleation of β-Mg_2Si is not dependent on the larger constituent phases and indicates that overall transformation kinetics is governed by bulk diffusion rates.

Keywords: aluminium; AlMgSi-alloys; homogenisation; precipitation; Mg_2Si; light optical microscopy; scanning electron microscopy; electrical conductivity

Citation: Hennum, E.; Marthinsen, K.; Tundal, U.H. Effect of Microstructure on the Precipitation of β-Mg_2Si during Cooling after Homogenisation of Al-Mg-Si Alloys. *Metals* **2024**, *14*, 215. https://doi.org/10.3390/met14020215

Received: 28 December 2023
Revised: 2 February 2024
Accepted: 6 February 2024
Published: 9 February 2024

1. Introduction

Advanced processing of aluminium alloys requires control of the secondary phases that form during thermo-mechanical processing like sheet rolling and extrusion [1,2]. Al-Mg-Si-alloys (AA6xxx alloys) are the most common Al extrusion alloys. 6xxx alloys are heat-treatable and precipitate-hardening alloys; the mechanical properties of the alloys are achieved by the formation of a fine distribution of nano-sized (metastable) precipitates formed during the final ageing process, after extrusion [3]. The processing route for extrusions is direct chill casting followed by homogenisation and then extrusion. The extrusion step involves three separate steps comprising pre-heating, extrusion, and quenching. The principle for conventional industrial extrusion of Al-Mg-Si alloys is a combined extrusion and solution heat treatment, referred to as "press heat treatment". During extrusion, the temperature is raised above the solvus by the heat generated by deformation. Appropriate quenching after extrusion retains the solid solution prior to ageing. Prior to the ageing step, the goal is to have as much of the alloying elements available for the final artificial ageing step.

For Al-Mg-Si alloys, cooling after homogenisation is a crucial step because the precipitation of the equilibrium β-Mg_2Si phase determines the processing capabilities in

subsequent steps, as well as the subsequent precipitation age hardening potential and, thus, the final properties [2–5]. It is therefore important to understand how microstructural variations affect the transformation of Mg_2Si during cooling.

In the literature [6–10], it is well established that the precipitation reaction during cooling of Al-Mg-Si alloys consists of two major reactions, a high-temperature reaction corresponding to the formation of the equilibrium phase, and a subsequent reaction caused by the formation of the metastable phases β′/B′. The β-Mg_2Si phase is well known to form on grain boundaries and constituent particles [6,9,11–13]. When precipitating in the grain interior, it forms plate-shaped particles. The metastable phase precipitates below ~400 °C, typically on dispersoids in alloys containing dispersoid-forming elements such as Mn and Cr [9,14,15]. Therefore, alloys with a high dispersoid density are more quench-sensitive [16–18]. Generally, the situation is more complex at lower temperatures, but the precipitating phase is usually interpreted as β′ or B′ but has also been shown to be of composite type [19].

However, despite previous thorough investigations and the fact that extensive experience has been accumulated through decades of industrial practice for the determination of acceptable process parameters for the extrusion of Al-Mg-Si alloys, our understanding of how Mg_2Si particles evolve during the different processing steps is still unsatisfactory. A kinetic model may aid this process by increasing the general understanding of the kinetics and also limiting the number of experiments required to establish a new practice. The main motivation for the present experimental work was to establish an experimental basis and understanding of the cooling stage after homogenisation that can serve as a foundation for the development of a kinetic model, which ultimately can be used directly or as part of a larger model suite to model the press heat treatment of Al-Mg-Si alloys. Some recent attempts to model precipitation reactions during cooling of Al-Mg-Si alloys are reported in [10,20,21].

The purpose of the experimental investigation was to determine the effect of the microstructure in terms of the level and distribution of presumed heterogeneous nucleation sites on the precipitation of β-Mg_2Si in balanced Al-Mg-Si alloys during cooling after homogenisation, with cooling rates comparable to typical post-homogenisation cooling rates applied in industry. The microstructural variations investigated are (i) the effect of iron content and alloys with similar effective solute contents of Mg and Si, and with three different levels of iron, namely 0.12, 0.20 and 0.28 wt.%. (ii) The effect of secondary dendrite arm spacing (DAS), realised by casting of billets with Ø203 and Ø95 mm, which results in different cooling rates and, thus, different DAS values. (iii) For comparison with high-purity alloys, two alloys were cast based on high-purity aluminium and no iron to produce conditions without primary phases and large grains. The different levels of iron content and their effects are also highly interesting from a recycling perspective as iron is an element that typically accumulates during recycling [22].

2. Materials and Methods

As a model alloy for these experiments, an alloy with a balanced Mg_2Si composition was chosen with 0.63 wt.% Mg and 0.36 wt.% Si. To investigate the effect of the number of primary phases, alloys with 0.12, 0.20 and 0.28 wt.% Fe were cast. Silicon lost to the primary Al-Fe-Si phases was compensated for according to the formula, in wt.%, $C_{eff}\ Si = C_{nom}\ Si - 0.25 \times C_{nom}Fe$ [1] to keep the effective Si level constant.

The key determining factor for the distribution of the primary phases is the secondary dendrite arm spacing (DAS), which is highly dependent on the solidification rate [23]. To create alloys with a smaller DAS and therefore denser distribution of primary phases, the alloys with different iron content were cast as billets with Ø203 and Ø95 mm. Additionally, two alloys were cast with high-purity aluminium as a base metal to create a completely iron-free material. One of the alloys was cast without grain refiner in order to have a material also free of grain refiner particles. Without iron, there are no primary phases to restrain grain growth, so the grains will grow to sizes in the order of millimetres during homogenisation

treatment. The purpose of these alloys was to have precipitation predominantly in the grain interior and thus to isolate this precipitation reaction.

The alloys were cast using standard direct chill gas-cushioned casting equipment at the Hydro Aluminium casting laboratory at Sunndalsøra. All alloys except the alloy VIG03 were cast with 0.5 kg/ton grain refiner to ensure a small and uniform grain size throughout the material. Prior to casting, 0.010 wt.% Ti was added to the casting furnace. All billets were homogenised at 575 °C for 2.25 h and subsequently water-quenched.

The measured chemical compositions of the alloy variants are listed in Table 1. The measurements were obtained with optical emission spectroscopy (OES) on the billet slices. Concentrations of trace elements such as Mn, Cu and Cr were all in the order of 10^{-4} wt.%. For unknown reasons, a substantially higher Ti content was measured for alloy FE-28-95 with OES on the billet slices, but the casting sample showed a similar value to the other alloys, and the billet slice OES measurement is therefore assumed to be incorrect.

Table 1. Overview of samples and their chemical composition.

Alloy	Ø [mm]	Fe [wt.%]	Mg [wt.%]	Si [wt.%]	Ti [wt.%]	Al [wt.%]
VIG03	95	0.00	0.62	0.36	0.00	99.00
FE-00-95	95	0.00	0.60	0.36	0.04	98.99
FE-12-95	95	0.12	0.63	0.40	0.02	98.79
FE-20-95	95	0.19	0.63	0.41	0.01	98.71
FE-28-95	95	0.28	0.62	0.43	0.08	98.55
FE-12-203	203	0.11	0.63	0.39	0.02	98.81
FE-20-203	203	0.19	0.63	0.40	0.02	98.73
FE-28-203	203	0.27	0.62	0.42	0.02	98.63

The β-Mg_2Si transformation was investigated with interrupted cooling experiments where the material was solution heat-treated by a 20 min hold at 540 °C after heating ~400 °C/h and then cooled at a constant cooling rate in the range of 1–6 K/min to different temperatures. The microstructure was characterised with light optical microscopy (LOM) and scanning electron microscopy (SEM) in addition to conductivity measurements. All samples were taken from the half-radius position of both the Ø203 mm and Ø95 mm billets to ensure the conditions were as equal as possible.

Samples selected for metallographic investigation were prepared with water-free suspensions and lubricants. For the polishing steps, lubricants with higher viscosity suitable for soft metals were used (Struers A 3/1 mu). The final polishing step was performed with ethanol-diluted (1:2) colloid suspension (OP-S). For area fraction measurements, a total area of 1.18 mm^2 was measured. Investigation with SEM was conducted with a Hitatchi SU6600. An acceleration voltage of 20 kV was used, and the working distance was ~7mm.

As a measurement of the overall precipitation reaction, electrical conductivity measurements were used. The electrical conductivity of aluminium is highly sensitive to the amount of elements in solid solution [24]. A precipitation reaction removes alloying elements from solid solution, which is measurable as an increase in electrical conductivity. The electrical conductivity of the samples was measured using a FISCHER Fischerscope MMS PC instrument with an eddy current probe. All samples were measured multiple times on both sides to minimise possible surface effects.

3. Results

3.1. Characterisation of Initial Structure

The grain sizes of the alloys with iron were measured at the centre, half-radius and outer positions of the billet using the standard line intercept method [25], and the results are presented in Figure 1. A total of 400 grains was measured for each sample. The grain size in the centre of the billet seems to decrease with increasing iron content, probably because of increased constitutional undercooling due to the higher alloying content. At the

half-radius and outer positions, the grain sizes seem to be less affected by the iron content and are relatively similar for both the Ø203 and Ø95 mm billets.

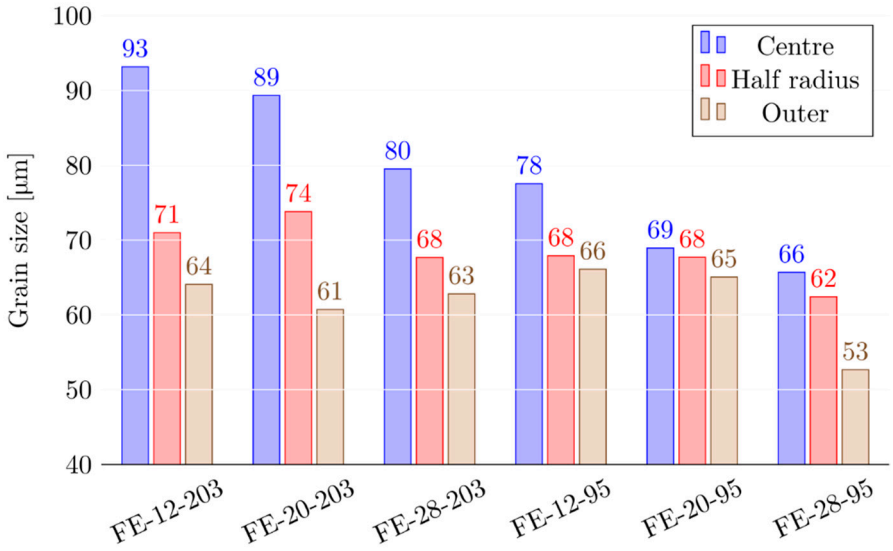

Figure 1. Measured grain sizes with the line intercept method for different casting diameters and iron levels.

The purpose of casting the smaller diameter, Ø95 mm, was to increase the solidification rate and thereby decrease the secondary dendrite arm spacing (DAS), which scales with the cube-root of time [23]. With a shorter DAS, the distance between the primary phases, which are often located along the secondary dendrite arms, decreases. In the Ø203 mm billets, typical values for the DAS were measured to be ~30, ~25 and ~20 µm in the centre, half-radius and outer position of the billet, respectively. For the Ø95 mm billets, the DAS was found to be ~15 µm in the mid-radius position.

The results from quantification of the amount of primary Al-Fe-Si phases by image analysis are shown in Figure 2. For a constant iron level, the measured volume fraction of the primary phases is similar within the experimental uncertainty for both casting diameters. The particle count statistics show a significantly higher number of primary phases in the Ø95 mm billets, as expected due to the increased solidification rate. Pores are common in cast material and arise from the casting process, e.g., the casting temperature. Micrographs (not shown) show that the all the cast material had a relatively high porosity level, which is not uncommon compared to industrial alloys. Most importantly, the porosity level seemed to be relatively similar in all alloys.

The purpose of using iron-free material was to have precipitation predominantly in the grain interior without the influence of grain boundaries and primary phases. In addition, this microstructure allows the observation of grain boundaries without the influence of primary phases. Without a sufficient number of larger particles, there are few obstacles to restrain the grain growth during homogenisation; thus, abnormal grain growth occurs. The resulting grain structures for alloys FE-00-95 and VIG03 are shown in Figure 3, showing millimetre-sized grains.

3.2. Iron Containing Alloys

Interrupted quench experiments for the alloys cast in Ø203 mm with three different iron levels were performed at cooling rates of 1, 2, 3 and 6 K/min. Quantification of the overall phase transformation was performed both with electrical conductivity and volume fraction measurements from quantitative analysis. Quantification based on electrical

conductivity was carried out by calculating a transformed fraction using the classical relation [26]

$$f = \frac{\sigma_1 - \sigma}{\sigma_1 - \sigma_0} \quad (1)$$

where σ_0 is the electrical conductivity of the solution heat-treated material (all Mg and Si in solid solution). σ_1 is the conductivity of the fully transformed material, obtained by slow cooling. In this experiment, a cooling rate of 10 K/hour (0.167 K/min) was used. For comparison with volume fraction measurements, quantification via electrical conductivity of the transformed fraction was calculated as

$$f = \frac{f_v}{f_v^{\max}} \quad (2)$$

where f_v is the volume fraction of a given specimen, and f_v^{max} is calculated from the densities of aluminium and Mg_2Si in Al.

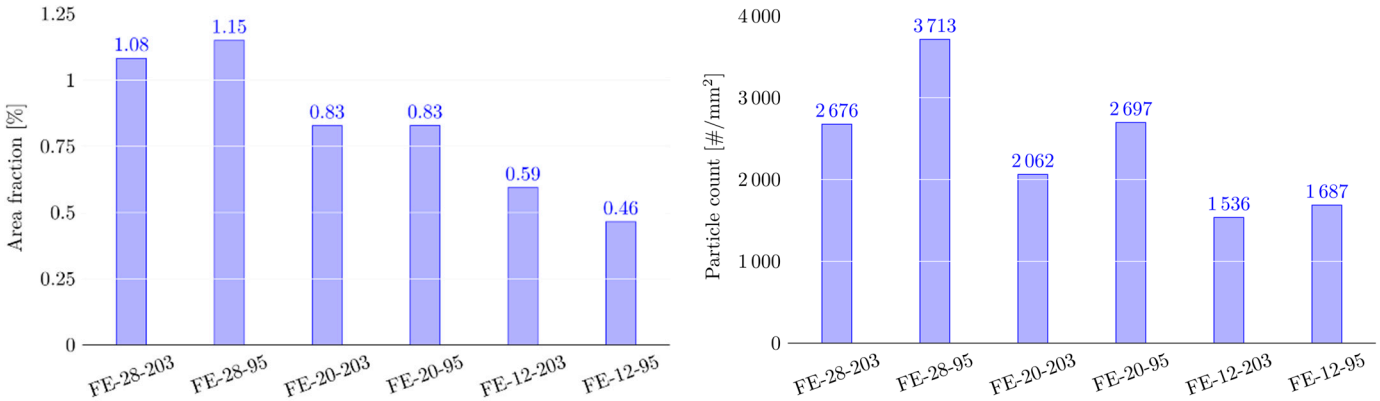

Figure 2. Quantification of primary Al-Fe-Si phases in iron containing alloys cast in Ø95 and Ø203 mm billets. Area fraction (**a**) and particle count statistics (**b**).

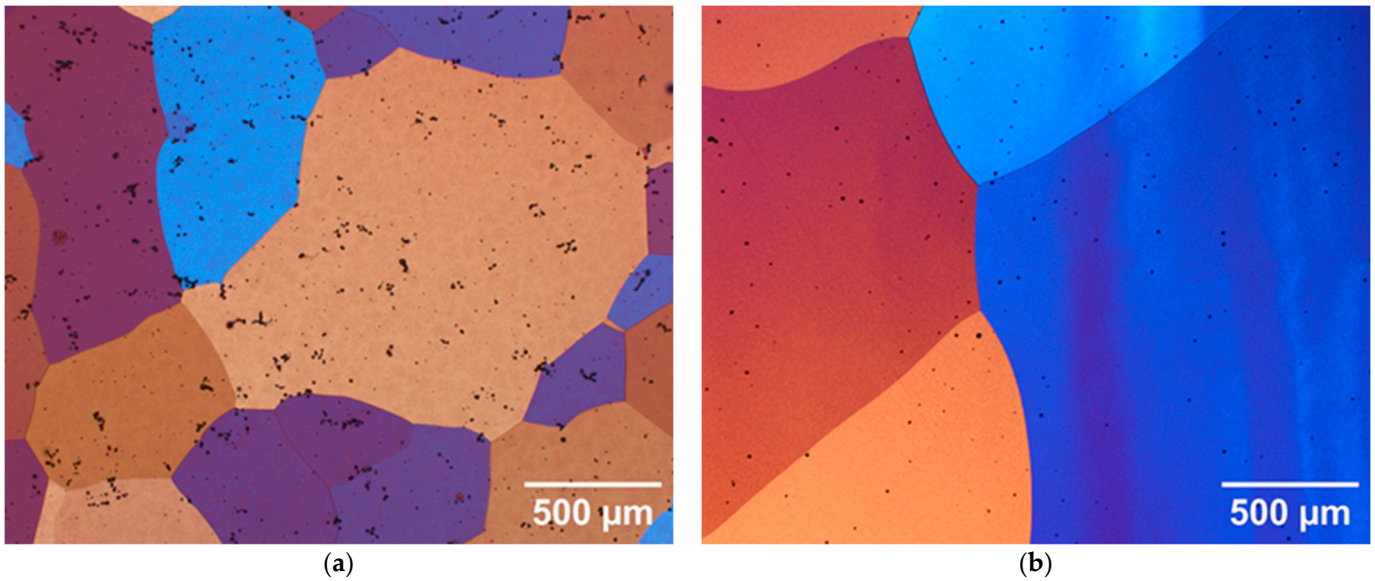

Figure 3. Grain structure in iron-free alloys FE-00-95 (**a**) and VIG03 (**b**) after homogenisation.

In Figure 4, the change in electrical conductivity vs. temperature for the investigated cooling rates is shown. Because the alloys exhibited an increase in conductivity from 540–500 °C during cooling, probably caused by further reduction of the iron solid

solution level, the zero level for conductivity change is chosen to be the value at 500 °C (solvus temperature).

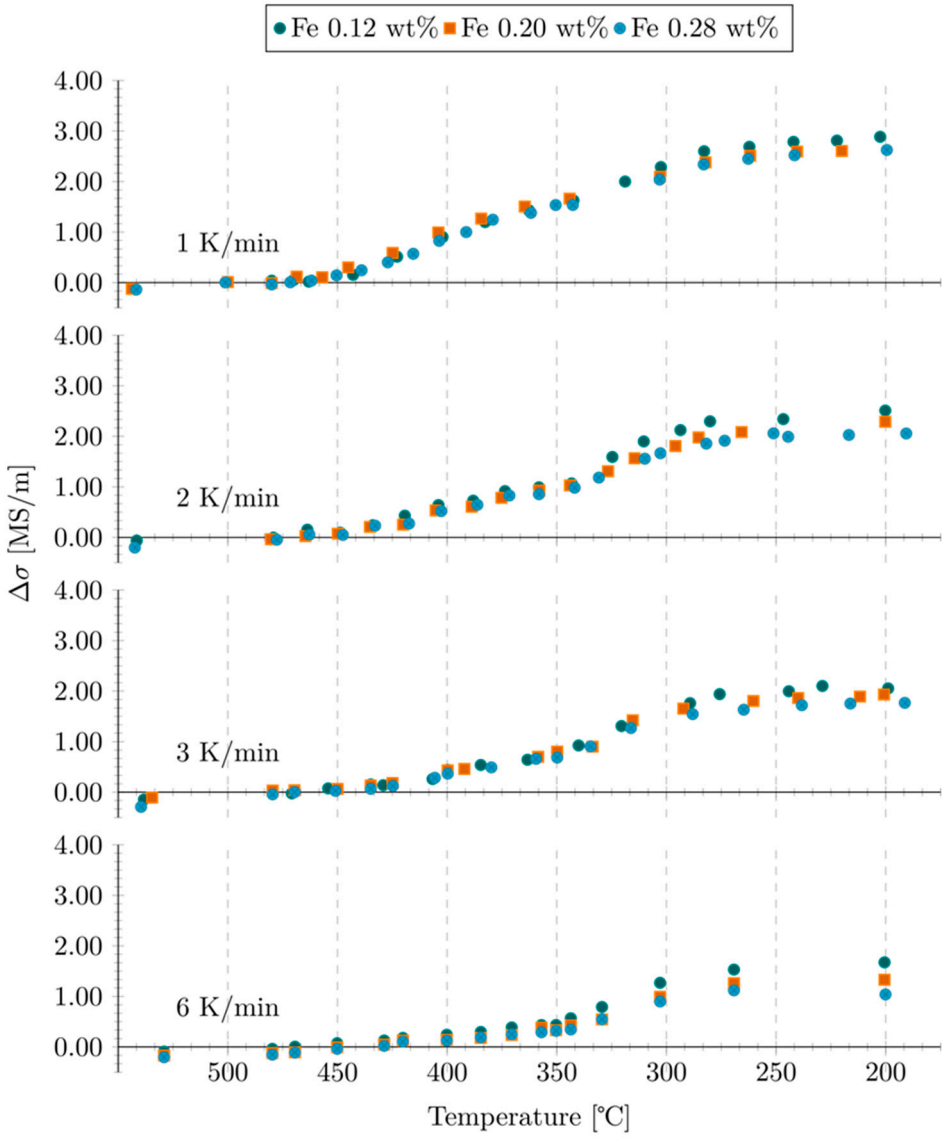

Figure 4. Change in electrical conductivity as a function of temperature for different cooling rates of 1, 2, 3 and 6 K/min and alloys with different iron content cast in Ø203 mm diameter.

In good agreement with well-established results for Al-Mg-Si alloys [6,8,9], two major reactions are identified. A high-temperature reaction starting slightly above 450 °C and a lower-temperature reaction below 350 °C. It is also immediately apparent from Figure 4 that the evolution of conductivity change vs. temperature is nearly identical in the three alloys. The electrical conductivity measurements show that the major onset of the phase transformation is around 450 °C. By investigating samples cooled to 470 °C, it was found that β-Mg_2Si had formed on coarse embedded impurities such as pores, grain refiner particles and primary phases already at this temperature.

From SEM micrographs of samples cooled to different temperatures (Figure S1), it was found that down to 420 °C, β-Mg_2Si particles are only found along grain boundaries and dendrite arms, often associated with primary phases. Faceted rod- and plate-like precipitates start to become visible in the grain interior at ~400 °C. At 380 °C, the intragranular particles have grown such that the bimodal nature of the β-Mg_2Si distribution becomes

apparent, as shown in Figure 5, showing the β-Mg_2Si particle distribution in Ø203 mm billets cooled at 1 K/min to 200 °C.

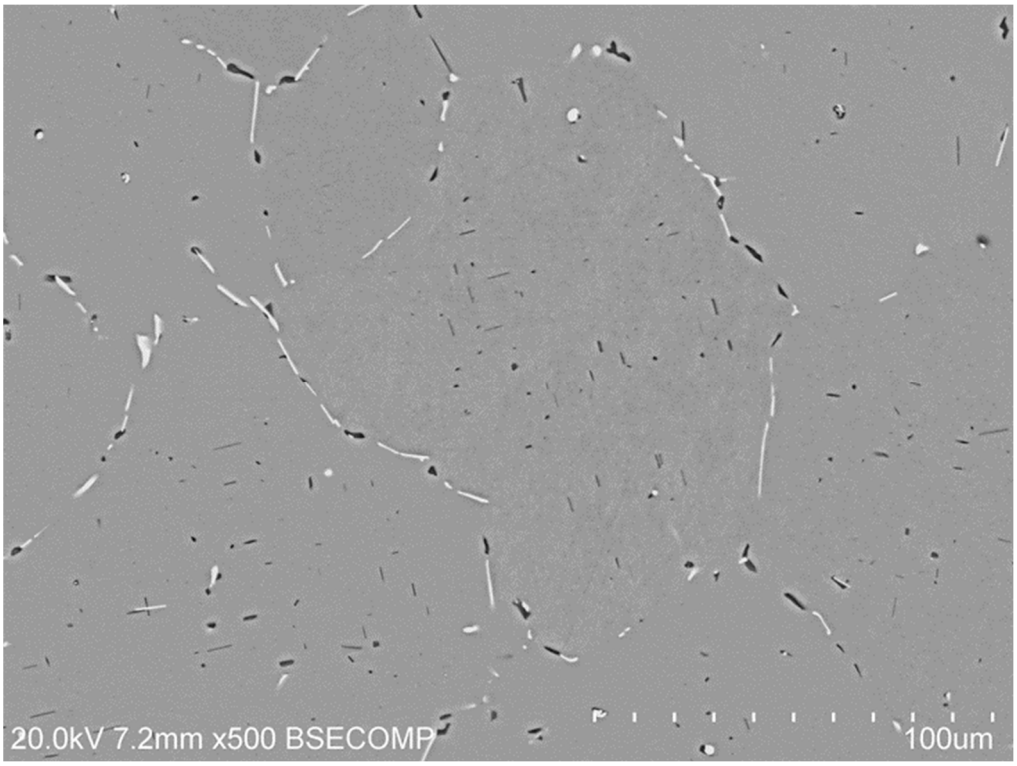

Figure 5. β-Mg_2Si (dark) particle distribution in Ø203 mm billets cooled 1 K/min to 200 °C.

From the microstructural investigation, it appears that the β-Mg_2Si transformation occurs in two stages with a minimum of two separate nucleation events. There is, however, no corresponding significant increase in the transformation rate observed in the electrical conductivity measurements, likely caused by the overlap of these reactions. Therefore, the exact onset of the intragranular precipitation reaction is difficult to determine, but the results suggest a nucleation temperature somewhere above ~400 °C, given that they also need some time to grow to observable sizes.

The results of the quantitative analysis of the optical microscopy images are shown in Figure 6. One of the major objectives of this experiment was to determine the effect of increased iron content. As already noted, the electrical conductivity measurements are close to identical for the three iron levels. A comparison of the transformed fraction calculated from the area fraction measurement and the conductivity measurement is shown in Figure 6. The transformed fraction from conductivity is taken from the value at 340 °C prior to the onset of the metastable precipitation reaction. There is a significant difference between the two values, with almost a factor-two difference for faster cooling rates. In this case, it is reasonable that the volume fraction β-Mg_2Si is underestimated, because the intragranular particles are hard to measure properly. The absolute values, however, indicate no particular difference between the three alloys in terms of volume fraction β-Mg_2Si (Figure 6). The particle size and count statistics displayed in Figure 7 also show no significant difference between the alloys.

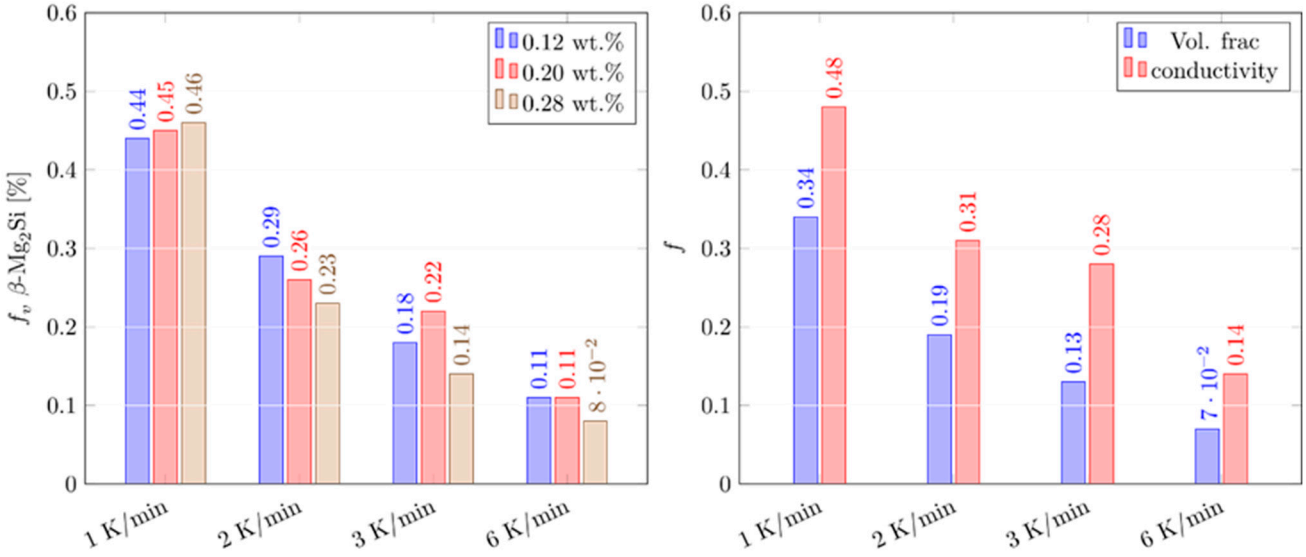

Figure 6. Quantification of the β-Mg_2Si transformation in the Ø203 mm billets. The left plot shows volume fraction measurements, while the right plot shows a comparison between transformed fractions calculated from conductivity and volume fraction measurements.

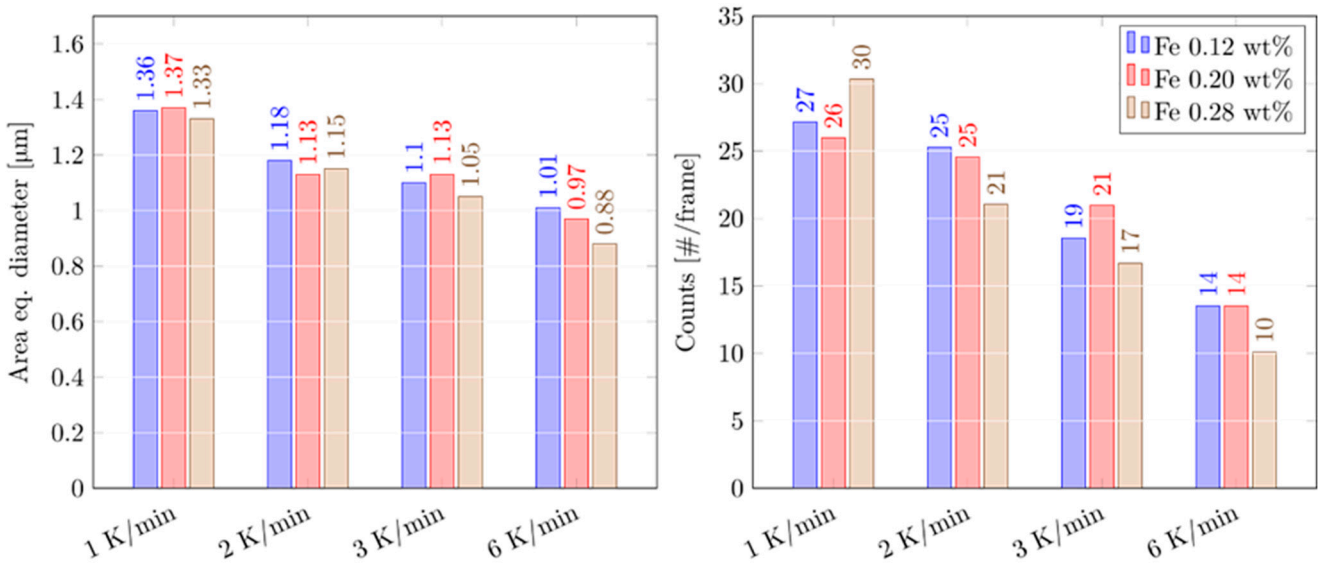

Figure 7. Particle statistics from quantitative image analysis for the Ø203 mm billets. The left plot shows the average diameter-converted areas, while the right shows the average number of particles counted in each frame.

With a more rapid solidification rate, the material cast in Ø95 mm material has a shorter DAS. As a result, the distance between the primary phases is reduced, leading to an overall denser distribution of potential nucleation sites for β-Mg_2Si. The hypothesis was that this would lead to more coarse particles forming as a result of an increased nucleation rate during the high-temperature onset.

Interrupted quench experiments for the Ø95 mm material were performed for the three iron-containing alloys at cooling rates of 1, 3, and 6 K/min. The evolution of the increase in electrical conductivity from a 500 °C level as a function of temperature for the different cooling rates is shown in Figure 8. As with the Ø203 mm billets, the onset of the major precipitation reaction is slightly above 450 °C. In this case, the conductivity measurements exhibited more noise, possibly explained by the fact that samples had to be taken from several billet slices.

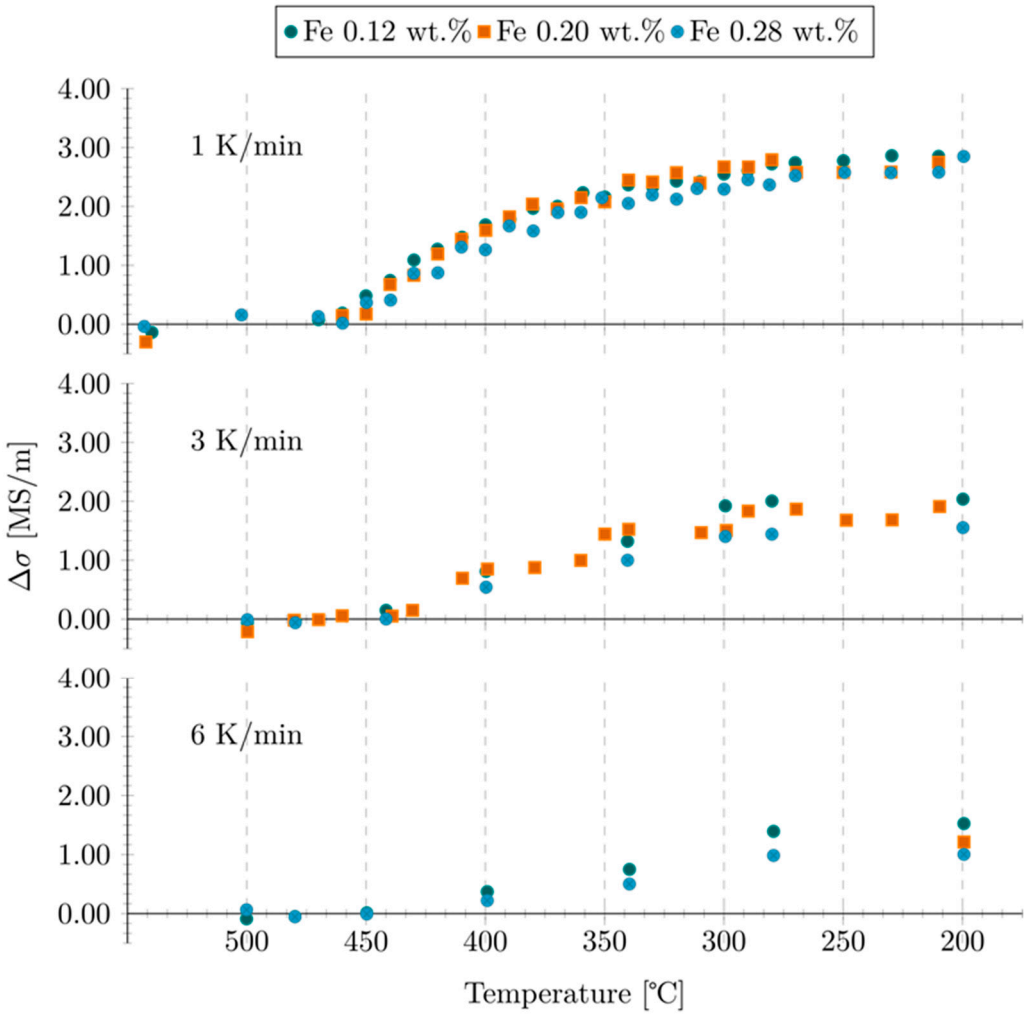

Figure 8. Change in electrical conductivity as a function of temperature for cooling rates of 1, 3 and 6 K/min and alloys with different iron content cast in Ø95 mm diameter.

SEM micrographs of the samples cooled to different temperatures (Figure S2) show that, compared to the Ø203 mm billets, the β-Mg_2Si particles appear coarser. Regions with intragranular β-Mg_2Si can be found, but these regions are much less prominent, indicating a suppression of intragranular β precipitation as compared to the Ø203 mm billets. Precipitation of the metastable phase is not so evident in the conductivity measurements shown in Figure 8 due to the increased noise and fewer data points. Still, a closer look at the data for alloy FE-12-95 (0.12 wt.% iron) cooled at 1 K/min shows an increase in conductivity at around 300 °C, indicating that a new precipitation reaction is triggered. This has also been confirmed from the SEM micrographs of this alloy.

The results from quantitative image analysis are shown in Figures 9 and 10. In accordance with the appearance of larger phases, a higher volume fraction of β-Mg_2Si is measured in the Ø95 mm compared to the Ø203 mm billets. They are also larger and there are fewer of them. In this case, the transformed fraction calculated from conductivity and volume fraction measurements agrees better, possibly explained by the larger size of the particles. In this case, there is neither any indication that the iron level has any impact on the β-Mg_2Si phase transformation during cooling, nor is there any significant difference between the alloys both in terms of volume fraction and particle statistics.

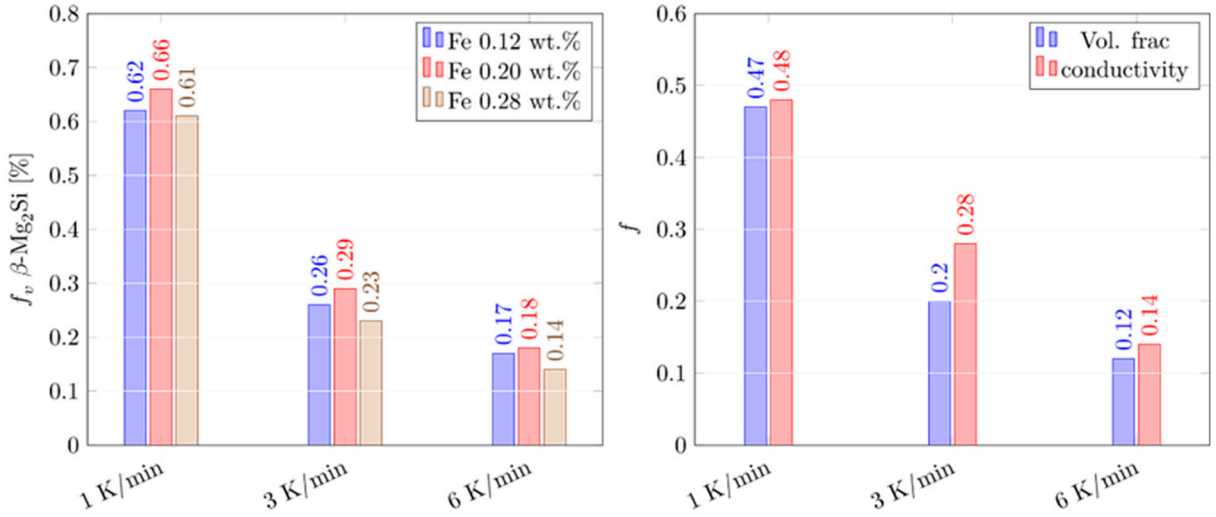

Figure 9. Quantification of the β-Mg_2Si transformation in the Ø95 mm billets. The left plot shows volume fraction measurements, while the right plot shows a comparison between transformed fractions calculated from conductivity and volume fraction measurements.

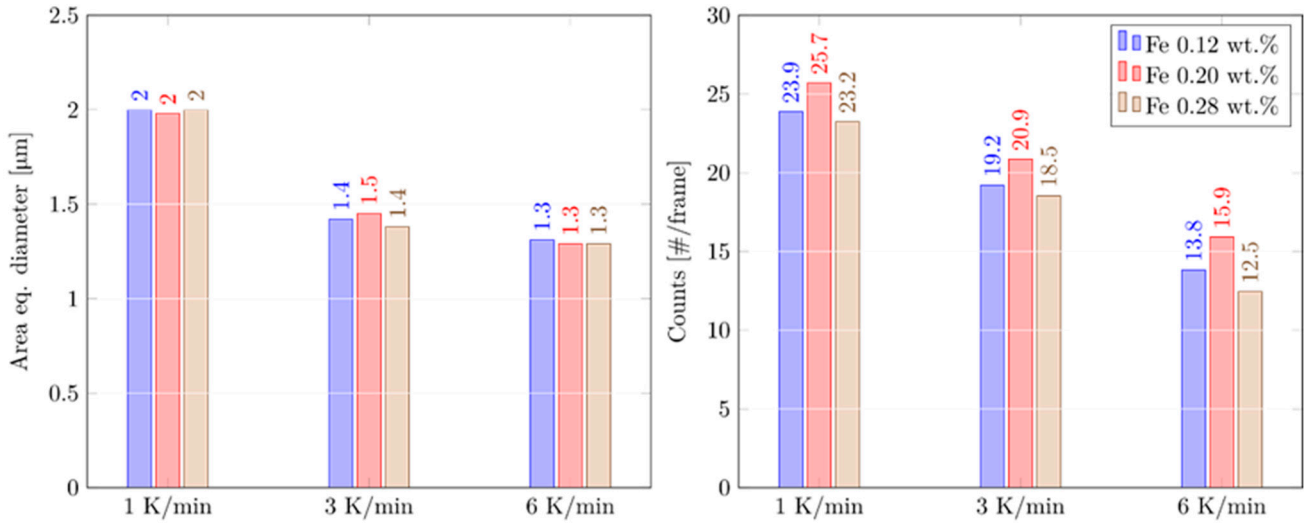

Figure 10. Particle statistics from quantitative image analysis for the Ø95 mm billets. The left plot shows the average diameter-converted areas, while the right shows the average number of particles counted in each frame.

Compared to the Ø203 mm billets, in accordance with the hypothesis formulated above, a shorter DAS in the Ø95 mm billets leads to a coarser β-Mg_2Si particle structure. However, despite measuring a higher volume fraction and density of primary phases, there are no indications from these results that the iron level has any impact on the precipitation of β-Mg_2Si phases during cooling.

3.3. Iron-Free Material

The purpose of the iron-free material was to investigate precipitation in the absence of primary phases and grain boundaries. For alloy FE-00-95, interrupted quench experiments were conducted for cooling rates of 1, 3 and 6 K/min. Based on the results for alloy FE-00-95, interrupted quench experiments were performed for alloy VIG03 in a homogenised state, but only for a cooling rate of 1 K/min. When comparing the results to the iron-free material, two interesting observations were made regarding similarities with the iron-containing alloys. Therefore, the results on the evolution of electrical conductivity vs. temperature

for the FE-00-95 alloy are plotted together with results from the Ø203 mm material in Figure 11. Evidently, the evolution of electrical conductivity is identical in the β-Mg_2Si transformation region of 350–450 °C. The only difference is the absence of the conductivity increase attributed to the precipitation of the metastable phase below 350 °C. A similar result was observed for the alloy VIG03 (without grain refiner) when comparing to alloys cast in Ø95 mm. (The electrical conductivity vs. temperature for alloy VIG03 is compared to alloy FE-12-95 in Figure S3). Also, in this case, the measurements show no significant difference between the alloys in the β-Mg_2Si transformation region.

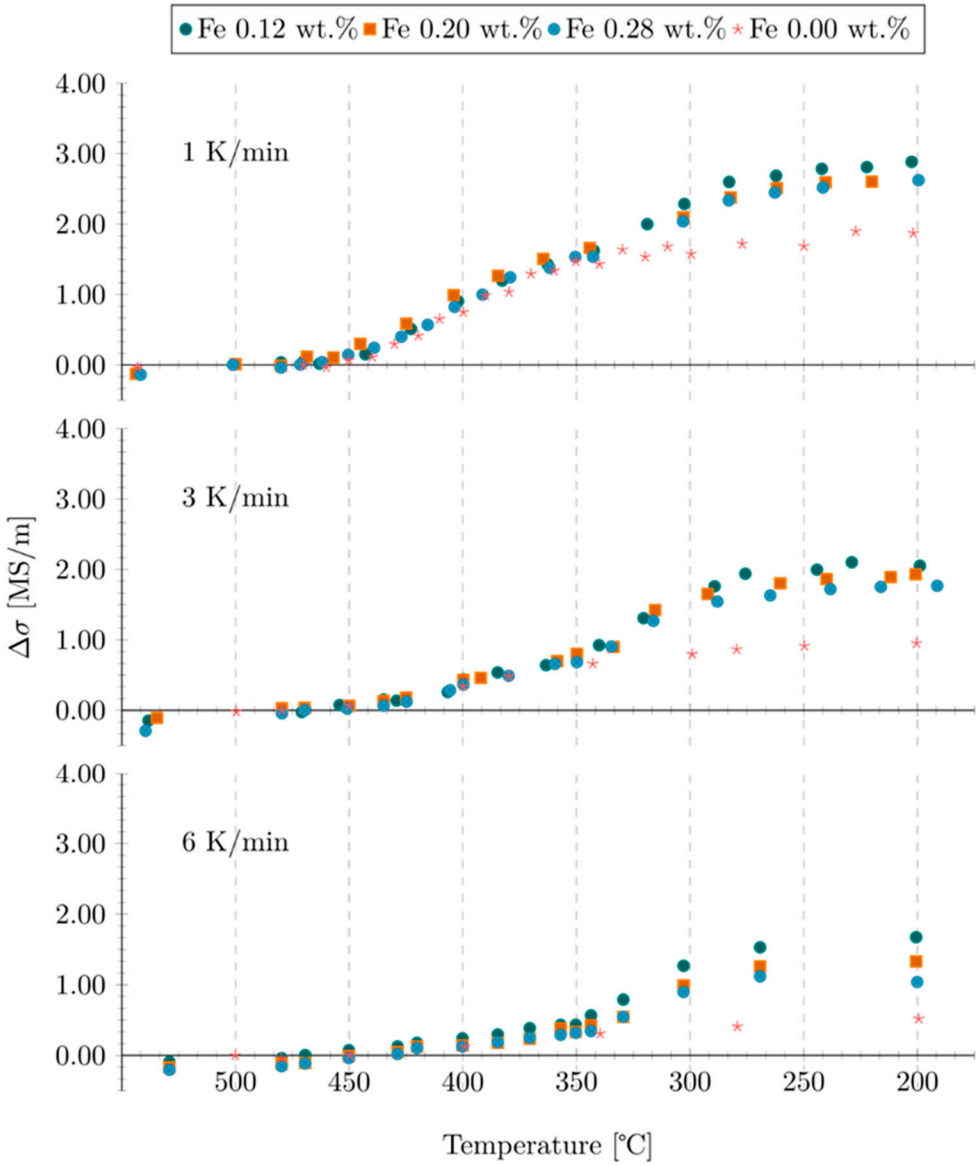

Figure 11. Change in electrical conductivity as a function of temperature for different cooling rates of 1, 3 and 6 K/min for alloys without iron (FE-00-95) and alloys with iron cast in Ø203 mm.

Metallographic investigations of the interrupted quench samples of alloy FE-00-95 have identified that β-Mg_2Si particles are formed as early as 470 °C on the embedded impurities. Further metallographic investigations (Figure S4) show that at 450 °C, β-Mg_2Si particles seemed to have formed exclusively on pores and grain refiner particles. At 430 °C, some plate-like precipitates are visible, and they increase in size and number density as the temperature decreases. Based on these results, the plate-like precipitates seem to nucleate at distinctly lower temperatures than particles forming on coarser heterogeneities;

they do, however, seem to form earlier than the intragranular particles described in the iron-containing alloys.

Images of the final microstructure (200 °C) for samples cooled at 1 K/min are shown in Figure 12a for alloy FE-00-95 and in Figure 12b for VIG03. In both cases, the precipitates are a mix of both irregularly shaped and faceted plate/rod-like precipitates in a seemingly random distribution. In both alloys, however, it is possible to find arrays or strings of precipitates. Clearly, this indicates that precipitation has occurred on heterogeneities to an extent much larger than the size of the precipitates. This is most prominent in the alloy VIG03, where the precipitate strings are indicated with arrows in Figure 12b. Possibly, the distribution of precipitates may be due to remnants of the underlying dendrite structure.

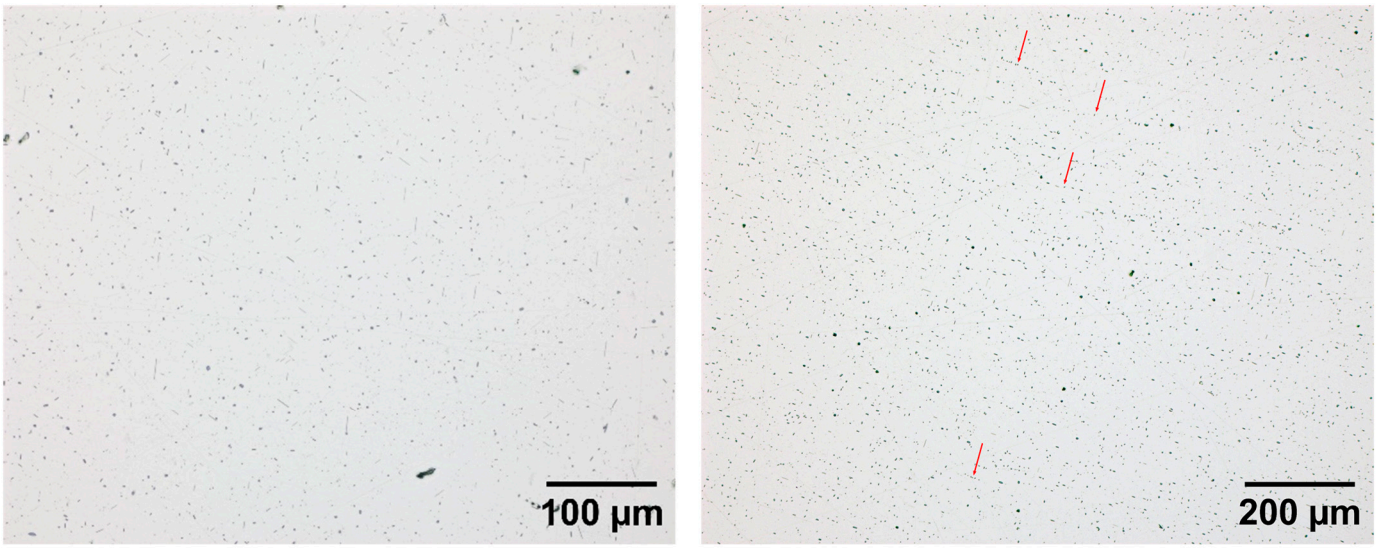

Figure 12. Light optical (LOM) micrographs showing distribution of β-Mg_2Si precipitates at 200 °C in (**a**) alloy FE-00-95 and (**b**) VIG03, cooled at 1 K/min. The red arrows indicate strings of precipitates.

The iron-free material allows for the investigation of precipitates forming on the grain boundaries without the co-location of primary phases. However, careful inspection of SEM images seems to indicate that the grain boundaries are not a particularly potent nucleation site compared to heterogeneities found elsewhere in the material.

The results for the volume fraction measurements are shown in Figure 13. In the absence of primary phases, it is easier to measure the area of individual β-Mg_2Si more correctly. Comparison of the transformed fraction calculated from volume fraction and conductivity measurements shows excellent agreement for temperatures above 340 °C. Below that, the values start to diverge, as shown in Figure 13c,d, where values are compared for different temperatures. Thus, it seems that the increase in conductivity below 340 °C is not due to the growth of β-Mg_2Si, but is instead an indication of the precipitation of metastable phases, which are not captured by the quantitative image analysis.

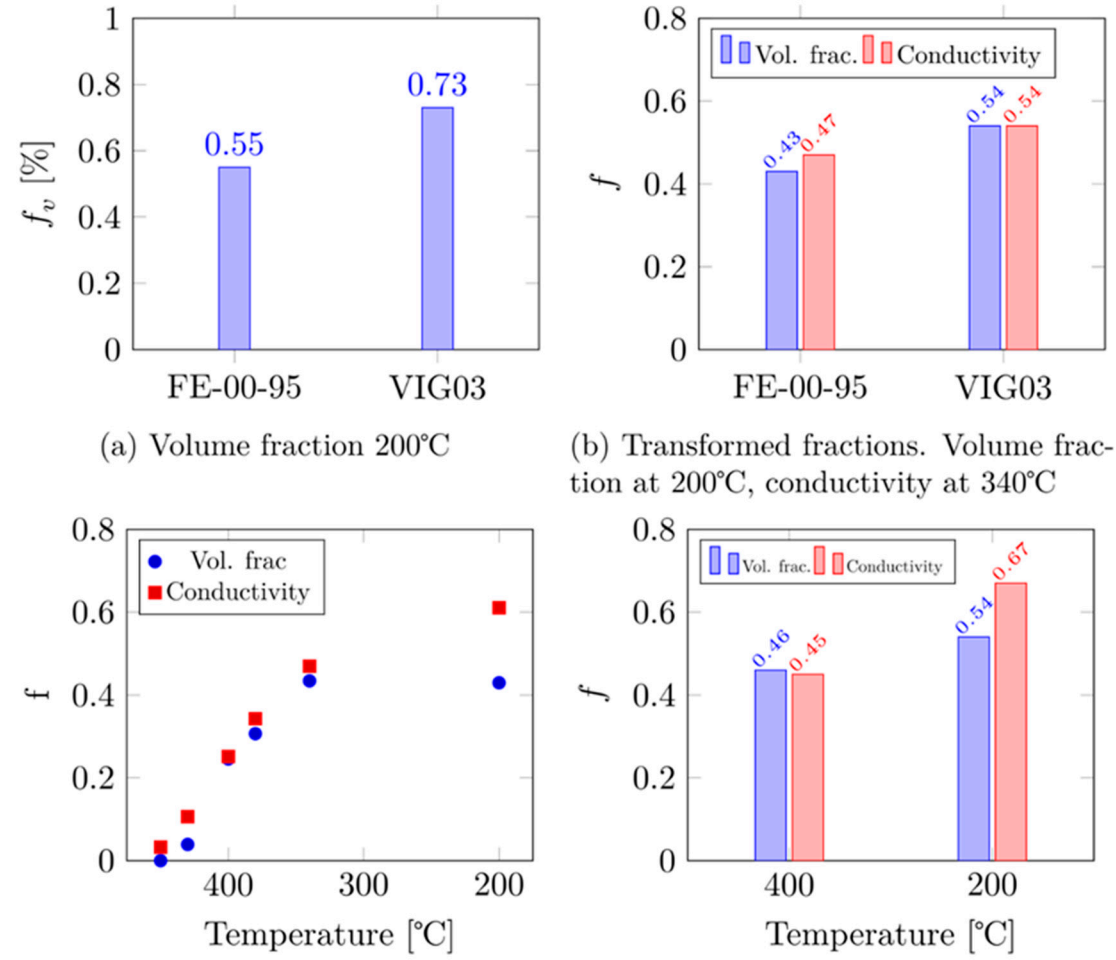

Figure 13. Quantification of phase transformation during cooling at 1 K/min for iron-free alloys FE-00-95 and VIG03 from quantitative image analysis and conductivity measurements (**a**,**b**). Both methods (**b**) agree well at temperatures above 350 °C. At lower temperatures, the transformed fraction from conductivity measurements is higher, indicating precipitation of smaller (metastable) phases (plot (**c**,**d**)).

4. Discussion

In these experiments, several different microstructures in terms of differences in density and distribution of presumed potential heterogeneous nucleation sites have been investigated with the purpose of identifying the effect of microstructure on β-Mg_2Si precipitation during cooling. From the standard nucleation theory, one might expect that the nucleation rate, and thus precipitation kinetics, increases with the number of potential nucleation sites. On this basis, the hypothesis was that the rate of transformation would increase with a shorter dendrite arm spacing (higher density of presumed nucleation sites). Comparing the transformed fraction between these two structures, as shown in Figure 14, it was indeed found that the transformation rate increases in this order.

However, no effect of increasing the number of constituent Fe-bearing particles on transformation kinetics was found in the iron-containing alloys. Additionally, the reaction onset temperatures and overall kinetics for β-Mg_2Si precipitation were found to be identical

in completely iron-free material. This raises many interesting questions regarding how microstructure impacts precipitation kinetics.

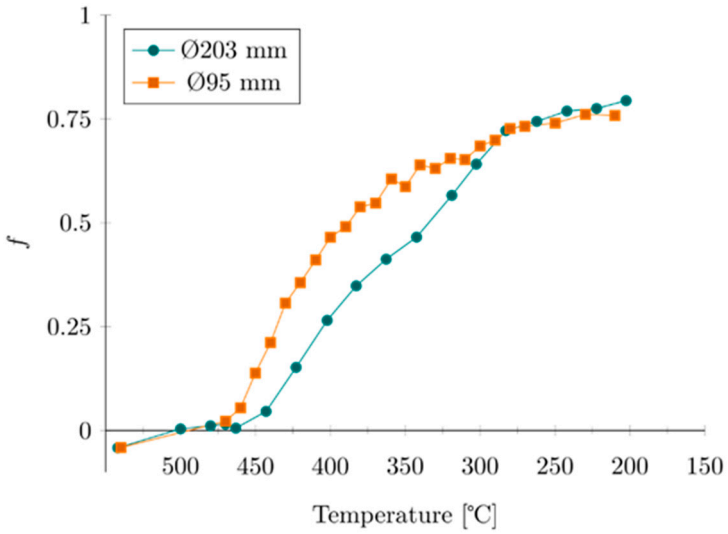

Figure 14. Transformed fraction as a function of temperature during cooling at 1 K/min for material cast in Ø203 mm and Ø95 mm with 0.12 wt.% iron.

The reason for investigating the effect of iron content is that Fe-bearing constituent phases are generally effective nucleation sites for secondary Mg-Si phases. In the comprehensive studies by Milkereit et al. [6,18], it was reported that all secondary β-Mg_2Si phases had seemingly nucleated on a constituent particle, even those located on grain boundaries. The presence of Mn- and Cr-bearing dispersoids is reported to refine the distribution of various secondary Mg- and Si-containing phases during cooling after homogenisation [9,12]. An increase in dispersoid density also leads to an increased quench sensitivity due to the promoted formation of non-hardening β′/B′ phases [16–18].

However, it is important to note that the relationship between the distance between potential nucleation sites and effective diffusion distances changes drastically as the temperature decreases during cooling. Generally, a one-to-one relationship between nucleation site and nuclei is not a common situation due to site saturation [27]. A significant increase in the number of constituent phases resulted from the increased iron content. However, their size and density increased in regions that already contain iron. Thus, a possible explanation for the lack of effect of iron content is that site saturation has already occurred at the lowest iron level (0.12 wt.%). The other possible explanation is that nucleation is not dependent on the larger Fe-bearing constituents.

The idea behind the iron-free alloys was to isolate intragranular precipitation of secondary Mg-Si phases. Possibly, different onset temperatures and particle distribution would result from the differences in the nucleation and growth conditions. Creating material completely free of embedded impurities with normal casting processes is difficult. The shared presence of pores, grain refiner particles and other inclusions, which provide a surface for substrate nucleation, is a possible explanation for the similar onset temperatures. The microstructure of alloy VIG03 was, in addition to not containing grain refiner particles, found to be relatively clean and seemingly free of impurities, which makes this explanation unlikely and points to other nucleation mechanisms. The same similarity between iron-containing and a pure ternary Al-Mg-Si alloy was also reported in [28], but explanations for this observation were not discussed.

In all crystals, an equilibrium level of dislocations is always present, and they are well-known nucleation sites for secondary Mg-Si phases [11,19]. Dislocations also develop due to thermal stresses during cooling. Investigation of the distribution of β-Mg_2Si phases in alloy VIG03 shows clear evidence that the equilibrium phase has formed along some forms of

boundaries in the material. A possible source of these boundaries is the imperfect merging of dendrite arms during solidification. Due to the mechanical load, the dendrites bend, and as a result, merge with a small misorientation [29]. In this regard, it is important to highlight an important difference between the two iron-free alloys FE-00-95 and VIG03. The former was cast with grain refiner, resulting in a uniform distribution of equiaxed grains of a relatively small size after casting. In the alloy VIG03, the individual grains and dendrites were allowed to grow more freely, resulting in longer dendrite boundaries. A speculation is that the subgrain/low-angle grain boundaries originating from the solidification process are the predominant nucleation sites for β-Mg_2Si in the iron-free alloys. It also possibly explains the difference between these alloys due to the differences in solidification characteristics. Only a slight difference in chemical composition was measured between the two iron-free alloys. In case this difference is responsible for the observed difference in precipitation kinetics, it indicates a very high sensitivity to variations in chemical composition.

It may be that embedded impurity particles, such as Fe-bearing constituents, are the most potent sites, but the comparison with the iron-free material in this study shows that there is obviously not a lack of nucleation sites for β-Mg_2Si without them. β-Mg_2Si on grain boundaries forms elongated particles up to 20 µm along the grain boundary direction, as seen in Figure 15. The presence of grain boundaries, in comparison with the iron-free material, evidently does not impact precipitation kinetics in the range of investigated cooling rates, but it does seem to have a significant effect on phase morphology. The differences in the distribution of β-Mg_2Si between the alloys indicate that there are different routes to the same precipitation kinetics. It therefore seems that precipitation of β-Mg_2Si is not a nucleation-limited reaction, and that the material quickly enters a stage controlled by volume diffusion (vacancy concentration), which is typical for many precipitation reactions [30].

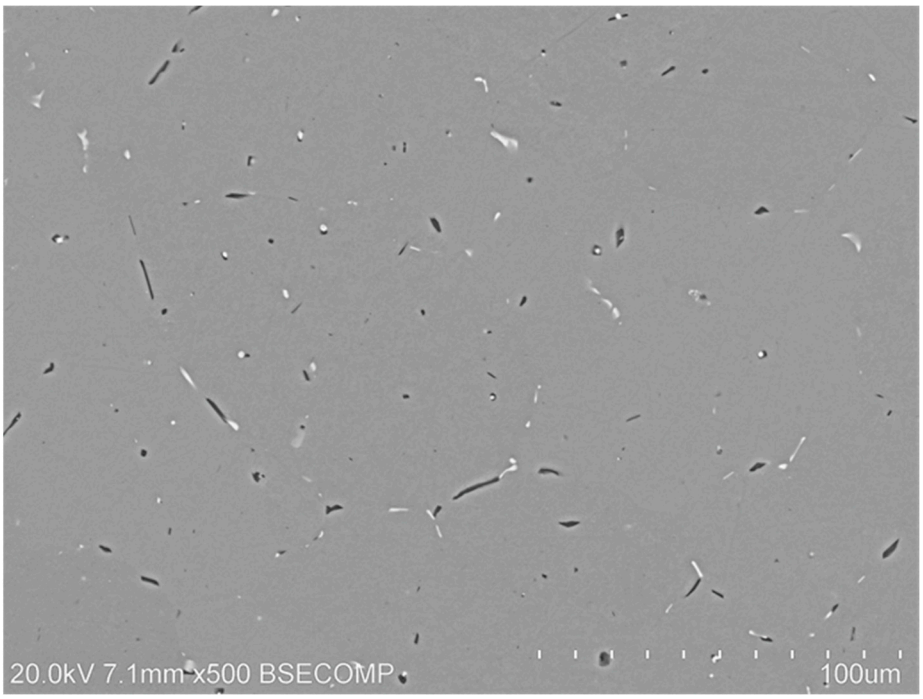

Figure 15. Distribution of β-Mg_2Si precipitates (dark) in alloy FE-28-203 after cooling to 200 °C.

5. Conclusions

In this experimental investigation, alloys with similar effective levels of alloying elements, but with different microstructures, have been investigated with the purpose of understanding how the density and distribution of potential nucleation sites affect the

precipitation of β-Mg_2Si during cooling after homogenisation. The main findings are summarised as follows:

- In the Ø203mm billets, the precipitation of β-Mg_2Si was characterised by precipitation at the grain and dendrite boundaries above 450 °C, followed by precipitation of intragranular β-Mg_2Si at a significantly lower temperature.
- With shorter secondary dendrite arm spacing, precipitation of intragranular β-Mg_2Si was suppressed to a large degree, leading to an overall coarser β-Mg_2Si structure.
- In iron-containing alloys, no effect of increased iron content on β-Mg_2Si precipitation was found.
- For iron-free alloys, the precipitation of β-Mg_2Si was found to be identical in terms of onset temperature and transformation kinetics to iron-containing alloys. In contrast to iron-containing alloys, no marked precipitation of the metastable phase was observed.

In agreement with other investigations, this study also identified the constituent Fe particles as potent nucleation sites for β-Mg_2Si. However, the comparison with the iron-free alloys revealed that nucleation is not dependent on the constituent phases. The results of this study suggest that site saturation occurs rapidly regardless of the microstructure, and that the kinetics of β-Mg_2Si precipitation is mainly controlled by bulk diffusion.

Supplementary Materials: The following supporting information can be downloaded at: https://www.mdpi.com/article/10.3390/met14020215/s1, Figure S1: SEM micrographs of the β-Mg_2Si particle structure at different temperatures during cooling at 1K/min in alloy FE-20-203 (0.20 wt.% iron); Figure S2: SEM micrographs showing the evolution of the microstructure during cooling 1 K/min. Alloy FE-12-95 (0.12 wt.% iron). The β-Mg_2Si phases are dark, and the primary Al-Fe-Si phases are bright; Figure S3: Change in electrical conductivity vs. temperature during cooling at 1 K/min for alloy FE-12-95 and VIG03; Figure S4: LOM micrographs of samples cooled to different temperatures at 1 K/min for the iron free alloy FE-00-95.

Author Contributions: E.H.: conceptualisation, investigation, formal analysis, methodology, visualisation, writing—original draft. K.M.: conceptualisation, methodology, supervision, writing—review and editing. U.H.T.: conceptualisation, methodology, supervision, review and editing. U.H.T. All authors have read and agreed to the published version of the manuscript.

Funding: This research received funding from the Research Council of Norway (RCN), project No. 290736 and project No. 309584.

Data Availability Statement: The original contributions presented in the study are included in the article/supplementary material, further inquiries can be directed to the corresponding author/s.

Acknowledgments: E. Hennum acknowledges the Research Council of Norway and Hydro Aluminium (where he is employed) for financial support. K. Marthinsen acknowledges funding from the Research Council of Norway through the Center for Research based Innovation SFI PhysMet.

Conflicts of Interest: Endre Hennum was partly funded by the Research Council of Norway (Grant No. 290736) through the funding scheme: Industrial PhD scheme—Doctoral projects in industry. Endre Asheim Hennum and Ulf Håkon Tundal are both employees of Hydro Aluminium (legal name: Norsk Hydro ASA). Hydro is a leading international aluminium and energy company with 32,000 employees in more than 140 locations and 40 countries. The funders had no role in the design of the study; in the collection, analyses, or interpretation of data; in writing of the manuscript; or in the decision to publish the results. The remaining author declare that the research was conducted in the absence of any commercial or financial relationships that could be construed as a potential conflict of interest.

References

1. Oddvin, R. Extrusion of AlMgSi Alloys. In Proceedings of the 9th International Conference on Aluminium Alloys, Brisbane, Australia, 2–5 August 2004; pp. 32–46.
2. Zhu, H.L.; Couper, M.J.; Dahle, A.K. Effect of Process Variables on Mg-Si Particles and Extrudability of 6xxx Series Aluminum Extrusions. *JOM* **2011**, *63*, 66–71. [CrossRef]
3. Sheppard, T. *Extrusion of Aluminium Alloys*; Kluwer Academic Publishers: New York, NY, USA, 1999.

4. Sun, Y.; Johnson, D.R.; Trumble, K.P.; Priya, P.; Krane, J.M. Effect of Mg_2Si Phase on Extrusion of AA6005 Aluminum Alloy. In *Light Metals 2014*; Springer: Cham, Switzerland, 2016; pp. 429–433.
5. Birol, Y. Precipitation during homogenization cooling in AlMgSi alloys. *Trans. Nonferrous Met. Soc. China* **2013**, *23*, 1875–1881. [CrossRef]
6. Milkereit, B.; Wanderka, N.; Schick, C.; Kessler, O. Continuous cooling precipitation diagrams of Al-Mg-Si alloys. *Mater. Sci. Eng. A-Struct. Mater. Prop. Microstruct. Process.* **2012**, *550*, 87–96. [CrossRef]
7. Birol, Y. The effect of homogenization practice on the microstructure of AA6063 billets. *J. Mater. Process. Technol.* **2004**, *148*, 250–258. [CrossRef]
8. Zajac, S.; Bengtsson, B.; Johansson, A.; Gullmann, L.O. Optimisation of Mg_2Si Phase for Extrudability of AA 6063 and AA 6005 Alloys. *Mater. Sci. Forum* **1996**, *217–222*, 397–402. [CrossRef]
9. Arnoldt, A.R.; Schiffl, A.; Höppel, H.W.; Österreicher, J.A. Influence of different homogenization heat treatments on the microstructure and hot flow stress of the aluminum alloy AA6082. *Mater. Charact.* **2022**, *191*, 112129. [CrossRef]
10. Falkinger, G.; Reisecker, C.; Mitsche, S. Analysis of the evolution of Mg_2Si precipitates during continuous cooling and subsequent re-heating of a 6061 aluminum alloy with differential scanning calorimetry and a simple model. *Int. J. Mater. Res.* **2022**, *113*, 316–326. [CrossRef]
11. Westengen, H.; Ryum, N. Precipitation reactions in an Aluminium 1-wt-percent Mg_2Si alloy. *Z. Fur Met.* **1979**, *70*, 528–535.
12. Qian, X.; Parson, N.; Chen, X.G. Effect of post-homogenisation cooling rate and Mn addition on Mg_2Si precipitation and hot workability of AA6060 alloys. *Can. Metall. Q.* **2020**, *59*, 189–200. [CrossRef]
13. Kahlenberg, R.; Wojcik, T.; Falkinger, G.; Krejci, A.L.; Milkereit, B.; Kozeschnik, E. On the precipitation mechanisms of β-Mg_2Si during continuous heating of AA6061. *Acta Mater.* **2023**, *261*, 119345. [CrossRef]
14. Rakhmonov, J.; Liu, K.; Rometsch, P.; Parson, N.; Chen, X.G. Effects of Al(MnFe)Si dispersoids with different sizes and number densities on microstructure and ambient/elevated-temperature mechanical properties of extruded Al–Mg–Si AA6082 alloys with varying Mn content. *J. Alloys Compd.* **2021**, *861*, 157937. [CrossRef]
15. Benarieb, I.; Puchkov, Y.A.; Sbitneva, S.V.; Zaitsev, D.V. Study of Decomposition of Supersaturated Solid Solution upon Quenching of Al–Mg–Si Alloy Sheets at Different Cooling Regimes. *Phys. Met. Metallogr.* **2023**, *124*, 901–907. [CrossRef]
16. Bratland, D.H.; Grong, O.; Shercliff, H.; Myhr, O.R.; Tjotta, S. Modelling of precipitation reactions in industrial processing. *Acta Mater.* **1997**, *45*, 1–22. [CrossRef]
17. Strobel, K.; Easton, M.A.; Sweet, L.; Couper, M.J.; Nie, J.F. Relating Quench Sensitivity to Microstructure in 6000 Series Aluminium Alloys. *Mater. Trans.* **2011**, *52*, 914–919. [CrossRef]
18. Milkereit, B.; Starink, M.J. Quench sensitivity of Al-Mg-Si alloys: A model for linear cooling and strengthening. *Mater. Des.* **2015**, *76*, 117–129. [CrossRef]
19. Qin, S.S.; Bendo, A.; Tsuchiya, T.; Lee, S.; Zou, Y.; Matsuda, K. Effect of Cooling Rate on Precipitation during Homogenization Cooling in Balanced Al-Mg_2Si Alloy. *Mater. Trans.* **2020**, *61*, 2115–2120. [CrossRef]
20. Du, Q.; Jia, L.; Tang, K.; Holmedal, B. Modelling and experimental validation of microstructure evolution during the cooling stage of homogenization heat treatment of Al–Mg–Si alloys. *Materialia* **2018**, *4*, 70–80. [CrossRef]
21. Miesenberger, B.; Kozeschnik, E.; Milkereit, B.; Warczok, P.; Povoden-Karadeniz, E. Computational analysis of heterogeneous nucleation and precipitation in AA6005 Al-alloy during continuous cooling DSC experiments. *Materialia* **2022**, *25*, 101538. [CrossRef]
22. Van den Eynde, S.; Bracquene, E.; Diaz-Romero, D.; Zaplana, I.; Engelen, B.; Duflou, J.R.; Peeters, J.R. Forecasting global aluminium flows to demonstrate the need for improved sorting and recycling methods. *Waste Manag.* **2022**, *139*, 231–240. [CrossRef] [PubMed]
23. Dantzig, J.A.; Rappaz, M. *Solidification*; CRC Press: Boca Raton, FL, USA, 2009.
24. Hatch, J.E. *Properties of Physical Metallurgy*; Aluminum Association Inc.: Arlington, VA, USA; ASM International: Almere, The Netherlands, 1984.
25. *ASM Hanbook: Materials Characterization*, 9th ed.; ASM International: Almere, The Netherlands, 1986; Volume 10.
26. Aaronson, H.I.; Masato, E.; Lee, J.K. *Mechanisms of Diffusional Phase Transformations in Metals and Alloys*; CRC Press: Boca Raton, FL, USA, 2010.
27. Kelton, K.G.; Lindsey, A. *Nucleation in Condensed Matter, Applications in Materials and Biolgy*; Elsevier: Amsterdam, The Netherlands, 2010.
28. Milkereit, B.; Starink, M.J.; Rometsch, P.A.; Schick, C.; Kessler, O. Review of the Quench Sensitivity of Aluminium Alloys: Analysis of the Kinetics and Nature of Quench-Induced Precipitation. *Materials* **2019**, *12*, 4083. [CrossRef] [PubMed]
29. Aveson, J.W.; Reinhart, G.; Nguyen-Thi, H.; Mangelinck-Noël, N.; Tandjaoui, A.; Billia, B.; Goodwin, K.; Lafford, T.A.; Baruchel, J.; Stone, H.J.; et al. Dendrite bending during directional solidification. In Proceedings of the 12th International Symposium on Superalloys, Seven Springs, PA, USA, 9–13 September 2012; pp. 615–624.
30. Starink, M.J. Analysis of nucleation and growth with the model for diffusion-controlled precipitation reactions based on the extended volume concept. *J. Alloys Compd.* **2015**, *630*, 250–255. [CrossRef]